Available online at www.sciencedirect.com

ScienceDirect

Ceramics International 40 (2014) 12485–12492

CERAMICS INTERNATIONAL

www.elsevier.com/locate/ceramint

Accounting for structural compliance in nanoindentation measurements of bioceramic bone scaffolds

Juan Vivanco[a,c,*], Joseph E. Jakes[b], Josh Slane[a,d], Heidi-Lynn Ploeg[a]

[a]Department of Mechanical Engineering, University of Wisconsin – Madison, 1513 University Avenue, Room 2258, Madison, WI 53706, USA
[b]Forest Biopolymer Science and Engineering, USDA Forest Service, Forest Products Laboratory, Madison, WI 53726, USA
[c]Facultad de Ingeniería y Ciencias, Universidad Adolfo Ibáñez, Viña del Mar, Chile
[d]Materials Science Program, University of Wisconsin – Madison, Madison, WI 53706, USA

Received 18 February 2014; received in revised form 11 April 2014; accepted 17 April 2014
Available online 1 May 2014

Abstract

Structural properties have been shown to be critical in the osteoconductive capacity and strength of bioactive ceramic bone scaffolds. Given the cellular foam-like structure of bone scaffolds, nanoindentation has been used as a technique to assess the mechanical properties of individual components of the scaffolds. Nevertheless, nanoindents placed on scaffolds may violate the rigid support assumption of the standard Oliver–Pharr method currently used in evaluating the Meyer hardness, H, and elastic modulus, E_s, of such structures. Thus, the objective of this research was to use the structural compliance method to assess whether or not specimen-scale flexing may occur during nanoindentation of bioceramic bone scaffolds and to remove the associated artifact on the H and E_s if it did occur. Scaffolds were fabricated using tricalcium phosphate and sintered at 950 °C and 1150 °C, and nanoindents were placed in three different (center, edge, and corner) scaffold locations. Using only the standard Oliver–Pharr analysis it was found that H and E_s were significantly affected by both sintering temperature and nanoindents location ($p < 0.05$). However, specimen-scale flexing occurred during nanoindentation in the 1150 °C corner location. After removing the effects of the flexing from the measurement using the structural compliance method, it was concluded that H and E_s were affected only by the sintering temperature ($p < 0.05$) irrespective of the nanoindent locations. These results show that specimen-scale flexing may occur during nanoindentation of components in porous bioceramic scaffolds or in similar structure biomaterials, and that the structural compliance method must be utilized to accurately assess H and E_s of these components.

Keywords: Bioceramic; Bone scaffold; Nanoindentation; Musculoskeletal injuries

1. Introduction

A common strategy for bone tissue regeneration is to implant porous three-dimensional scaffolds which, once implanted at the defect site, are required to provide mechanical and biological functions, ultimately integrating with surrounding native tissue. The mechanical environment requires the scaffold to offer appropriate strength and stiffness while providing adequate space for bone cells and their cell–cell communication. One of the key micro-environmental aspects affecting cell differentiation is the base material of the scaffold and its interaction with cells. Common biomaterials used as bone replacement are those made of inorganic materials such as calcium phosphate (CaP) based bioceramics [1]. CaP scaffolds have been also designed to mimic nanoscale properties of natural bone tissue such as crystalline structure and morphology [2]. Among CaP bioceramics, hydroxyapatite (HA, $Ca_{10}(PO_4)_6(OH)_2$) and tricalcium phosphate (TCP, $Ca_3(PO_4)_2$) are the most commonly used in clinical applications because of their biocompatibility, osteoconductivity, osteoinductivity, bioactivity, bioresorbability, and their chemical similarity to the mineral phase of bone [3–5].

*Corresponding author at: Department of Mechanical Engineering, University of Wisconsin – Madison, 1513 University Avenue, Room 2258, Madison, WI 53706, USA. Tel.: +1 608 262 2690; fax: +1 608 265 2316.
E-mail address: vivanco@wisc.edu (J. Vivanco).

http://dx.doi.org/10.1016/j.ceramint.2014.04.103
0272-8842/

Previous work has shown that the nanoscale mechanical properties of bioceramic scaffolds such as stiffness and nanoporosity influence the scaffold's bioactivity [6,7]. More recently Moroni and co-workers have shown that at the micro- and nanoscale, physical and biological functionalities influence the bone regenerative capacity of bioceramic scaffolds [8].

Nanoindentation has become a powerful non-destructive testing technique for evaluating the mechanical properties of porous structures such as CaP bioceramics [9–11] and trabecular bone [12–15]. In nanoindentation testing, a probe is pressed into and withdrawn from a material following a prescribed loading profile. During the test, both load and displacement are recorded. From the resulting load–depth trace, mechanical properties, most often Meyer hardness and elastic modulus, can be directly assessed. One of the most widely used methods to assess Meyer hardness and elastic modulus from nanoindentation load–depth traces is the standard Oliver and Pharr (O–P) method [16]. However, the O–P method assumes the material tested is rigidly supported in the nanoindentation test machine. When this assumption is not satisfied the utility of O–P analysis becomes compromised. For instance, when the specimen flexes or has heterogeneities, such as free edges or interfaces between regions of dissimilar properties, artifacts may arise in the properties assessed using the O–P analysis. Fortunately, Jakes and co-workers recently developed the structural compliance method to remove these types of artifacts [17–19]. They found that the effect of both specimen-scale flexing and edges nearby nanoindents is to introduce an additional compliance into the experiment. This compliance, termed the structural compliance, behaves similar to the machine compliance and a modified SYS (Stone, Yoder, Sproul) correlation [20] can be used to quantify the structural compliance. The load–depth trace can then be corrected using the structural compliance in the same manner the usual machine compliance correction is applied. Finally, the O–P method can be performed on the corrected load–depth trace.

Sintering, a well-known manufacturing method to fabricate bioceramics [21], has been observed to be an important determinant of their microstructural and physical characteristics [7,22,23] which influence the scaffold's capacity to induce bone formation [24]. Although extensive research has been done concerning bioceramic scaffolds for use in bone tissue engineering applications, a comprehensive study to determine the influence of sintering temperature on mechanical properties of CaP-based scaffolds is still warranted [7,25]. Nanoindents can be placed on individual scaffold struts to assess the mechanical properties of CaP. However, if the strut flexes under loading, the rigid support assumption of the O–P method will be violated. Thus, the aim of this study was to use the structural compliance method [19] to assess whether or not specimen-scale flexing can occur during nanoindentation of bone scaffolds and to remove the associated artifacts in the nanoindentation results if flexing occurs. In this study beta-TCP (β-TCP) scaffolds manufactured at two different sintering temperatures were studied.

2. Materials and methods

Samples were fabricated by Phillips Plastic Corporation (Hudson, WI, USA) [26] and sintered at target temperatures of 950 °C and 1150 °C in air using a heating scheme described briefly elsewhere [27]; beginning at room temperature the scaffolds were heated at a rate of 1 °C/min to 600 °C, soaked at 600 °C for 1 h, heated to either 950 °C or 1150 °C using a heating rate of 2 °C/min, and finally held at the target temperature for 5 h. Samples were subsequently cooled to 600 °C at a rate of 5 °C/min and finally furnace cooled to room temperature. The scaffolds consisted of six approximately 500 μm^2 beams stacked upon one another in orthogonal directions to form a porous cubic structure (~5 mm^3). Fig. 1 shows representative stereomicroscope images of a sintered bioceramic scaffold used in the current study. Specimens used for nanoindentation testing were first mechanically ground using 600, 800 and 1200-grit silicon carbide grinding paper in ascending order (Allied High Tech Products Inc, Rancho Dominguez, CA, USA) for approximately 1–2 min per step. After grinding, samples were mechanically polished using 1, 0.25 and 0.05 μm diamond suspensions in descending order (MetaDi Polycrystalline, Buehler, Lake Bluff, IL, USA) for 30–60 s per step. After each successive step, samples were washed and sonicated in distilled water to remove debris material from the sample surface. After sonification, alcohol was applied to the sample and immediately dried under a warm air source.

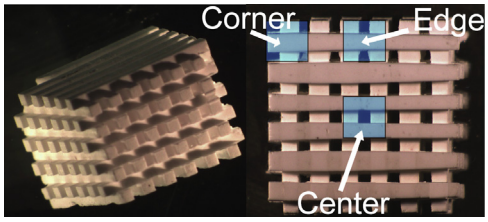

Fig. 1. Stereoscope image of a representative sintered bioceramic scaffold after completion of the sintering process. Different indentation regions are indicated as well: (1) corner, (2) edge, and (3) center. Each scaffold was approximately 5 mm^3.

The microstructural morphology of the scaffold surface was analyzed by scanning electron microscopy (SEM) whose images were obtained with a LEO DSM 1530 field emission SEM (Zeiss-LEO, Oberkochen, Germany) operated at 5 kV Fig. 2. SEM images were analyzed with an image analysis software package ImageJ, NIH, USA). The average grain diameters were calculated using the linear intercept method (ASTM E 112-88) from a total of six measurements for each scaffold. Physical properties such as volume, density, and porosity were determined using Archimedes' principle, a fluid displacement method, using a 70% ethanol solution as explained elsewhere [23].

A Hysitron TI 950 TriboIndenter (Hysitron Inc., Eden Prairie, MN, USA) equipped with a diamond Berkovich probe was used to perform all nanoindentation testing. Standard methods were used to calculate the machine compliance and area functions (based on contact stiffness) by performing a series of 100 indents on a fused silica standard with loads ranging from 0.2 to 10 mN. Based on this series of indents, the machine compliance was determined to be 0.75 nm/mN. All testing was conducted under ambient laboratory conditions

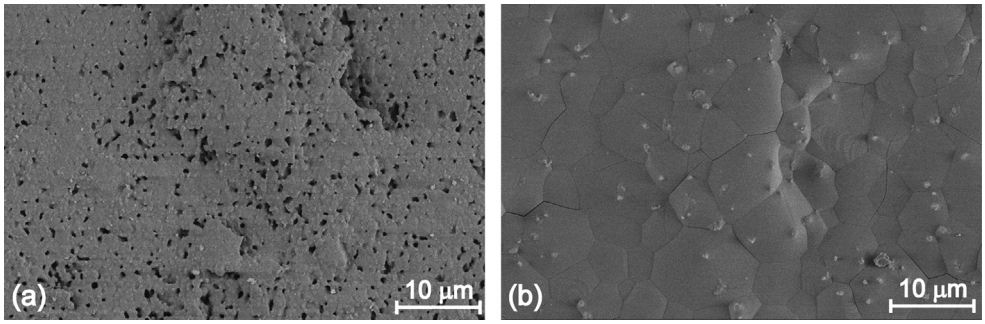

Fig. 2. SEM micrographs of the morphology of the cross sections of β-TCP bone scaffolds sintered at different temperatures: (a) 950 °C and (b) 1150 °C.

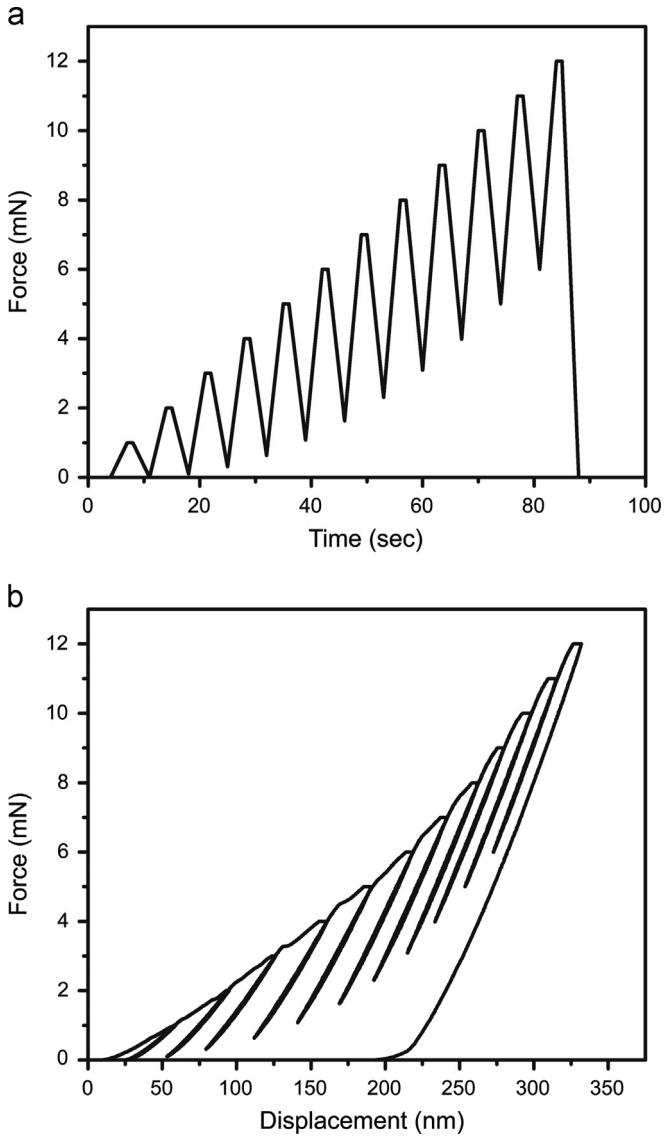

Fig. 3. Representative (a) load profile and (b) force–displacement data from the 1150 °C sintered scaffold evaluated in the center region.

(~23 °C, 52% relative humidity). The thermal drift rate measured before each test averaged 0.1 nm/s. Load–depth traces were corrected for both machine compliance and thermal drift prior to structural compliance analysis.

A single scaffold from each sintering temperature was used for nanoindentation testing. For each scaffold, nanoindentation was performed on individual struts in three different regions: corner, edge, and center (Fig. 1). To construct the SYS correlation to assess C_s, load control multi-load indents were conducted, which consisted of loading segments, holds at the partial load, and unloading segments with load increasing for each cycle (Fig. 3). The current research tests consisted of 12 steps ranging from 1 mN to 12 mN with a total duration of 90 s comprising loading and unloading segments of 3 s and hold segments of 1 s. Series of five ($n=5$) partial unload nanoindents were conducted in the center of a strut in corner and edge locations whereas a series of 14 ($n=14$) nanoindents were conducted in the center of a strut in the center region. All nanoindents were placed in the center of the struts and based on the analysis of Jakes and Stone the free edges of the struts' edges will not have an effect on these nanoindents [17]. In-situ scanning probe microscope (SPM) images were obtained using the Berkovich probe and nanoindent locations were selected from these images (Fig. 4). SPM images of residual nanoindent impressions were also obtained for quality assurance. Surface roughness for each scaffold was also measured from SPM images with values of 40.3 ± 4.3 nm and 6.0 ± 1.5 nm, for the 950 °C and 1150 °C scaffolds, respectively. To minimize the effects of surface roughness and uncertainties in zero depth on the analysis, partial loads from 1 to 3 mN were excluded. Young's moduli (E_s) of the different scaffolds were calculated using Eq. 4 (see Section 3), where E_d and ν_d are the properties of the diamond probe, 1140 GPa and 0.07 respectively. The value of Poisson's ratio used for TCP scaffold materials, ν_s, was assumed to be 0.27 [28].

All results are expressed as means and standard deviations. A two-way analysis of variance (ANOVA) was performed using the statistics package MiniTab 14 (MiniRab Inc., State College, PA, USA) to investigate the influence of the sintering temperature (2 levels: 950 °C, 1150 °C) and surface location (3 levels: corner, edge, center) on hardness (H) and elastic modulus of the sample (E_s). Assumptions of normality and equality of variance were checked by Anderson–Darling Normality test and F-test, respectively. Uncertainty of the structural compliance (C_s) was determined by least squares analysis of linear fit. In all cases the significance level was set at $\alpha=0.05$.

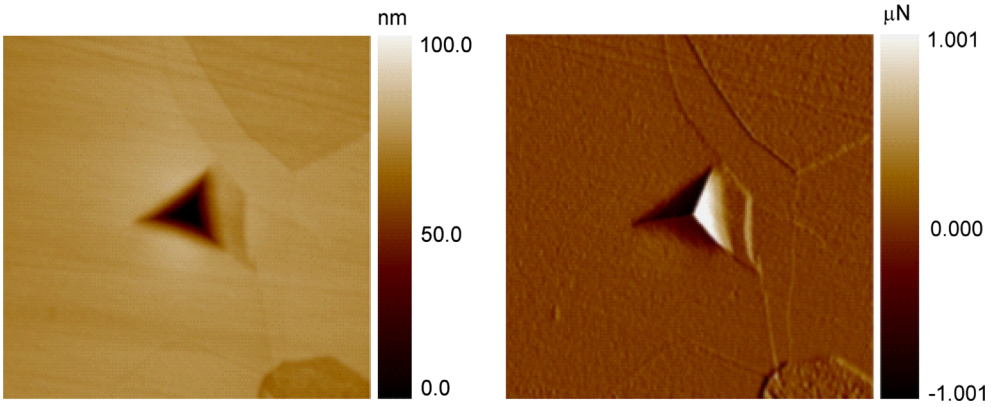

Fig. 4. Lateral force in situ-SPM image of nanoindent in 1150 °C sintered scaffold strut.

3. Theory/calculation

Meyer hardness (H) is a metric of a material's resistance to plastic deformation and is defined as

$$H = \frac{P_0}{A_0} \tag{1}$$

where P_0 and A_0 are the maximum load and contact area, respectively, immediately prior to unloading. In the O–P method [16] A_0 is estimated using a calibrated area function and the contact depth

$$h_c = h_0 - \varepsilon P_0 C_p \tag{2}$$

where h_0 is the depth immediately prior to unloading, ε a geometric factor equal to 0.75 for a Berkovich probe, and C_p is the contact compliance defined as the inverse of the initial unloading slope in a load–depth trace that has been corrected for both machine compliance (C_m) and structural compliance (C_s). The "effective" modulus of contact is

$$E_{eff} = \frac{1}{C_p A_0^{1/2}} \tag{3}$$

and for indentation against a homogenous, isotropic, elastic half-space

$$\frac{1}{E_{eff}} = \frac{1}{\beta}\left(\frac{1-\nu_s^2}{E_s} + \frac{1-\nu_d^2}{E_d}\right) \tag{4}$$

where E_s and E_d are Young's moduli and ν_s and ν_d are Poisson's ratios of specimen and indenter, respectively. β is a numerical factor which here is assumed to be $2/\pi^{1/2} = 1.128$.

The O–P analysis is contingent on an accurate load–depth trace. In addition to the standard machine compliance (C_m) correction, which removes the portion of the measured depth attributed to the flexing of the load frame, the flexing of the ceramic scaffold itself must also be considered. Jakes and coworkers developed the structural compliance method to identify this type of specimen-scale flexing and remove its contribution from the measured depth [17–19]. In the structural compliance method, the modified SYS correlation is used and given as

$$C_t {P_0}^{1/2} = C_s {P_0}^{1/2} + J_0^{1/2} \tag{5}$$

where $J_0 = H/E_{eff}^2$ is the Joslin–Oliver parameter [29] and C_t is the compliance assessed from an unloading segment that has been corrected for C_m. C_t can be assessed as a function of load from a single location using a multiload indent. A plot of $C_t {P_0}^{1/2}$ as a function of ${P_0}^{1/2}$ forms a straight line of slope C_s if J_0 and C_s are independent of load. The intercept, $J_0^{1/2}$, is an area-independent material parameter that represents the ratio $H^{1/2}/E_{eff}$. After C_s is assessed, its contribution to the depth can be removed in the same manner as the C_m correction and the usual O–P method can be performed on the corrected load–depth trace.

4. Results and discussion

SEM micrographs of TCP scaffolds sintered at 950 °C and 1150 °C are shown in Fig. 2. The micrographs show clear demarcation in the grain boundary, grain sizes and micropores. In the current study, it was found that the higher sintering temperature resulted in significantly larger grain sizes (Fig. 2) and higher degree of densification (p-value < 0.05). Scaffold grain sizes increased from 0.74 ± 0.04 μm to 8.07 ± 0.20 μm whereas material density increased from 2.27 ± 0.15 g/cm^3 to 3.22 ± 0.29 g/cm^3, for sintering temperature of 950 °C and 1150 °C, respectively.

Meyer hardness and elastic modulus for scaffolds fabricated at 950 °C and 1150 °C sintering temperatures were assessed on struts in the center, edge, and corner regions. Initially, H and E_s were evaluated from the final 12 mN unloading segment in the multiload nanoindent using the standard O–P analysis (Eqs. 1–4), which assumes that the strut is rigidly supported. For the 950 °C sintering temperature, H and E_s were not significantly different among the indent regions (Fig. 5); however, for 1150 °C sintering temperature H and E_s evaluated in the corner location were significantly lower (p-value < 0.05) than the edge and center locations (Fig. 5 and Table 1).

Structural compliance was assessed using SYS correlations in which the slope, C_s, and the intercept, $J_0^{1/2}$, were obtained for each multi-load indent according to Eq. 5. Fig. 6 shows representative SYS correlations for each sintering temperature and measurement location. The high slope of the corner SYS

correlation in the 1150 °C sintered specimen indicates a large C_s in this region. All the indents in this region had a consistently high C_s (Fig. 7). This suggests that the strut was not rigidly supported beneath the nanoindents and flexed under loading, similar to a cantilever with a point load applied towards its end. It could be that the nanoindent location on the strut was beyond the final supporting strut in the layer below or that a failure occurred between the top strut and ones below. The values of the SYS correlation intercepts, which represent

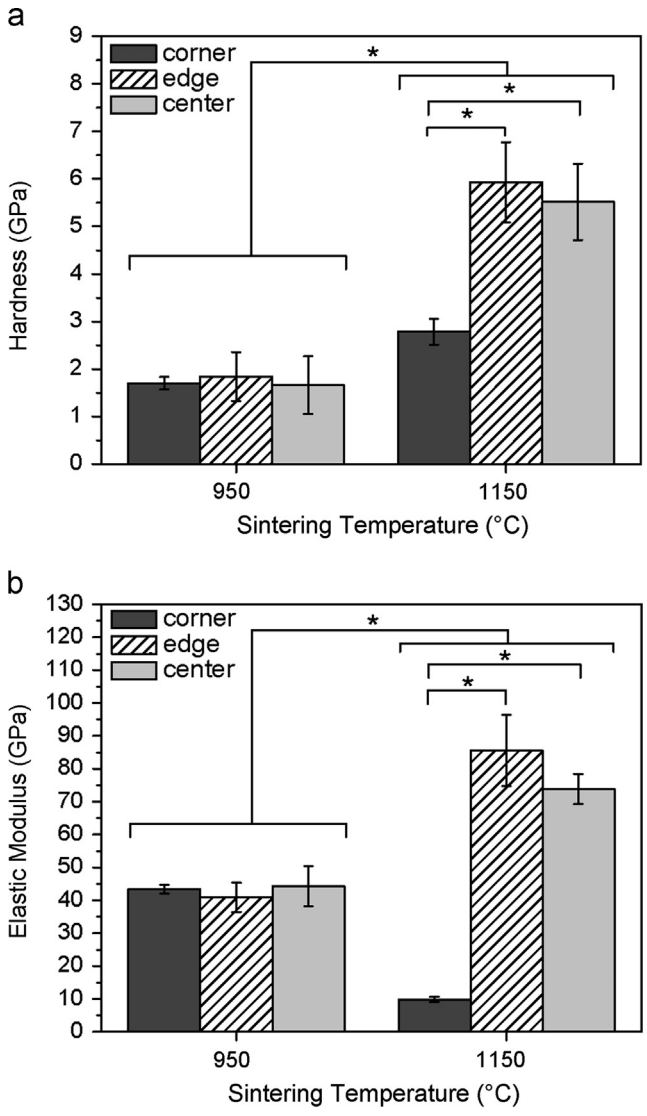

Fig. 5. Mechanical properties of TCP scaffolds directly calculated using the standard O–P analysis without accounting for C_s: (a) hardness, (b) elastic modulus (*P-value < 0.05). Error bars represent standard deviations.

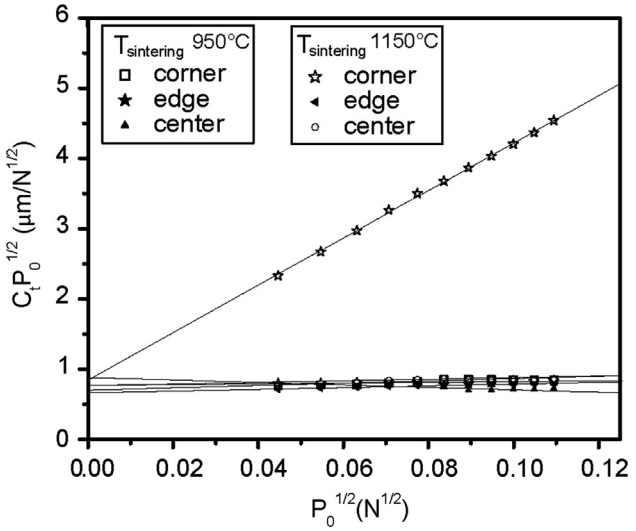

Fig. 6. Representative SYS correlations for each region in TCP scaffolds.

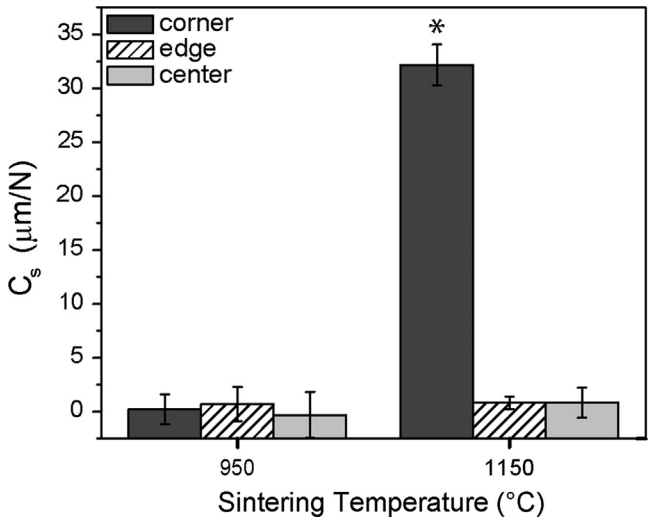

Fig. 7. Structural compliance, C_s, evaluated at different locations on TCP scaffolds (*P-value < 0.05). Error bars represent standard deviations.

Table 1
Nanomechanical properties evaluated at a maximum applied force of 12 mN at different locations for TCP scaffolds sintered at 950 and 1150 °C. Locations: corner (n=5), edge (n=5), and center (n=14). Values are expressed in average ± standard deviation.

T sintering (°C)	Region	$J_0^{1/2}$ (μm²/N)	C_s (μm/N)	Standard O–P method		O–P method after C_s correction	
				E_s (GPa)	H (GPa)	E_s (GPa)	H (GPa)
950	Corner	0.81 ± 0.15	0.23 ± 1.40	43.38 ± 1.39	1.70 ± 013	46.28 ± 10.23	1.71 ± 0.15
	Edge	0.81 ± 0.10	0.71 ± 1.58	40.90 ± 4.44	1.84 ± 0.52	46.33 ± 11.06	1.86 ± 0.54
	Center	0.81 ± 0.18	-0.30 ± 2.14	44.31 ± 6.17	1.66 ± 0.61	46.92 ± 20.98	1.67 ± 0.66
1150	Corner	0.94 ± 0.08	32.19 ± 1.88	9.84 ± 0.75	2.79 ± 0.27	78.31 ± 4.58	5.29 ± 0.49
	Edge	0.72 ± 0.05	0.84 ± 0.58	85.65 ± 11.56	5.93 ± 0.85	99.00 ± 14.72	6.05 ± 0.86
	Center	0.79 ± 0.12	0.84 ± 1.38	73.86 ± 4.85	5.52 ± 0.80	87.13 ± 20.42	5.65 ± 0.96

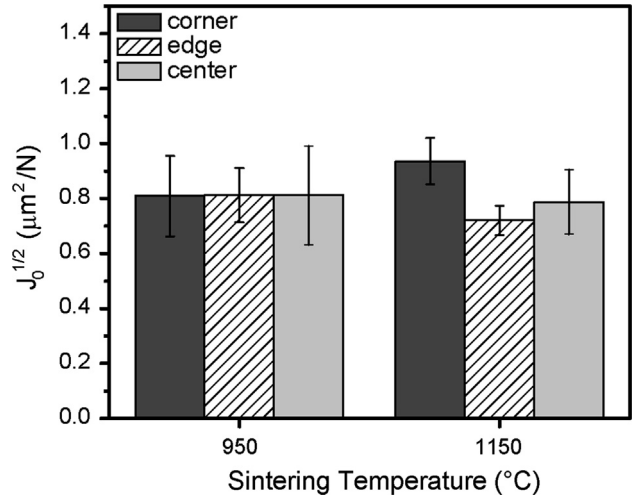

Fig. 8. Material parameter $J_0^{1/2}$ evaluated at different locations on TCP scaffolds. Error bars represent standard deviations.

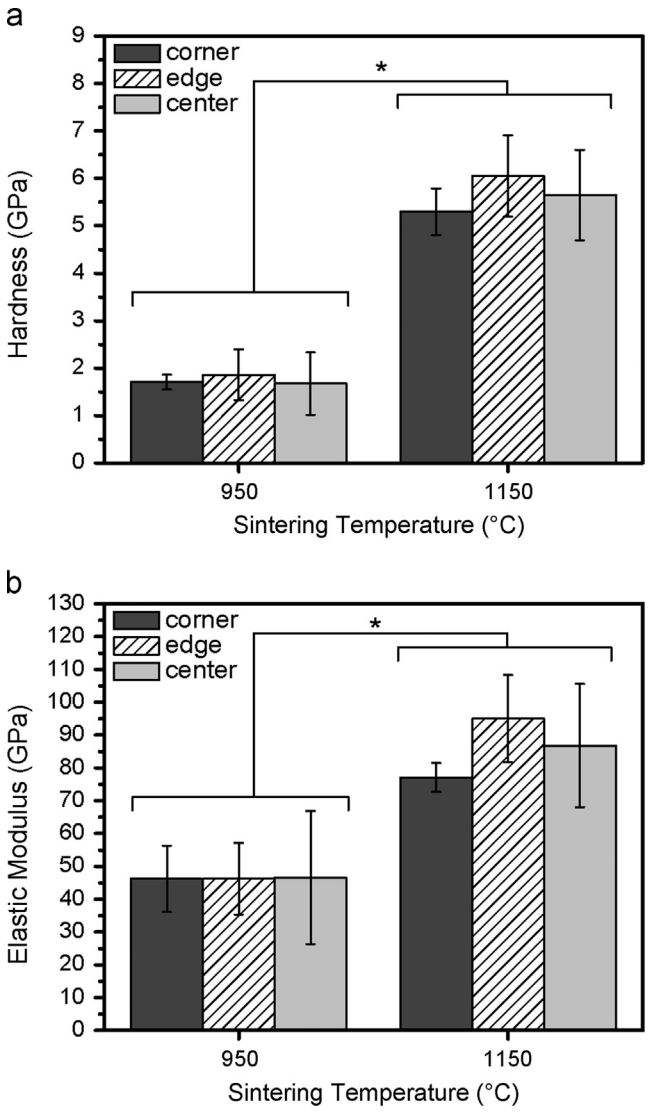

Fig. 9. Mechanical properties of TCP scaffolds after taking into account structural compliance, C_s, in data analysis: (a) hardness, (b) elastic modulus (*P-value < 0.05). Error bars represent standard deviations.

the material parameter $J_0^{1/2} = H^{1/2}/E_{\text{eff}}$, are in Fig. 8. There were no statistically significant differences in $J_0^{1/2}$ found between the locations within each sintering temperature or between the two temperatures.

After correcting each load–depth trace for the structural compliance assessed from the corresponding SYS correlation, the final 12 mN unloading segments were reanalyzed with the O–P method (Fig. 9). The correction increased H and E_s in the 1150 °C corner location and revealed that the mechanical properties of the β–TCP bioceramic scaffolds did not significantly vary over different locations. Additionally, it was verified that both H and E_s were significantly affected by the sintering temperature (p-value < 0.05), where mechanical properties of the scaffold fabricated at 950 °C were significantly lower than those at 1150 °C (Fig. 9).

Combining both sintering conditions, ANOVA analysis showed that surface location was not statistically significant, with p-values of 0.107 and 0.109 for H and E_s, respectively. Even for each sintering temperature taken separately, there was not a significant difference between corner, edge, and center locations for both H and E_s. Thus, the differences observed on the mechanical properties of β–TCP bioceramic scaffolds were only due to sintering process and not by the location of the nanoindents as in the case of using the standard O–P method without the structural compliance method.

The increase in mechanical properties with sintering temperature is in consonance with reported studies of similar CaP based bioceramic materials [9,10,27]; the lower the sintering temperature, the smaller the grain size and the higher the volumetric fraction of grain boundary phase. Hence, a rise of sintering temperature resulted in an increase of grain size in the microscale regime and so less grain boundary phase was observed, which resulted in higher hardness and elastic modulus of β-TCP bioceramic scaffolds.

Although the results obtained after using the C_s correction have more variability than those obtained from the standard O–P method (Table 1), they are considered more accurate because they remove the systematic artifacts associated with specimen-scale flexing. The increased variability, especially in E_s, is primarily from the uncertainties in assessing C_s from the slope of the SYS correlations. The variability in SYS correlations is higher in the β-TCP bioceramic than in previous work in fused silica and (100)-oriented silicon wafers [19]. The slope of the SYS correlation is a straight line and equal to C_s assuming that $J_0^{1/2} = H^{1/2}/E_{\text{eff}}$ and C_s are independent of load. Because the grain sizes in the β-TCP bioceramic are comparable to the size of the nanoindents [27], it is possible that as the nanoindent grows during the partial loading and unloading cycles of the multiload indent nearby grain boundaries can randomly affect the overall elastic responses and yielding processes beneath the nanoindentation probe. This could cause an indentation size effect and $J_0^{1/2}$ to somewhat vary as a function of load and contribute to uncertainties in C_s. Also, indentation size effects in H or E_{eff} arising from surface roughness, polishing effects, or strain gradient plasticity [30] could also affect the calculated value of C_s. However, the straight line fits of the SYS correlations in Fig. 6 support that indentation size effects are

small. Furthermore, the presence of the large C_s in the corner of the 1150 °C sintered scaffold is obvious despite the variability observed in assessing C_s. As previously mentioned, when results were interpreted directly from the standard O–P method, without considering the artifact of C_s, difference between the H and E_s of the indent locations in the 1150 °C would have been more than 100% (Table 1). But by implementing the structural compliance method it could be verified that the differences observed in the mechanical properties of β-TCP bioceramic scaffolds fabricated in the range of 950 °C to 1150 °C were only due to sintering temperatures and not due to the location of the nanoindent. Although in the current study nanomechanical properties were evaluated over different locations of only a single scaffold, in a previous related bioceramic study we found repeatability and consistency of physical and macromechanical properties over $n=50$ samples [31].

5. Conclusions

Nanoindentation offers a non-destructive method for determining the mechanical properties of brittle and fragile bioceramics used in biomedical applications. In this study, the structural compliance method was used to assess whether or not specimen-scale flexing occurs during nanoindentation of bioceramic bone scaffolds and to remove the associated artifact on H and E_s if it did occur. Struts in bioceramic scaffolds can flex under loading during nanoindentation and if ignored the hardness (H) and elastic modulus (E_s) values will be artificially low. The recently developed structural compliance method can be used to assess the structural compliance (C_s) arising from flexing and remove its effect from the nanoindentation load–depth trace. The corrected load–depth trace can then be analyzed with the O–P method in the typical manner. We evaluated H and E_s in the center, edge, and corner regions of β–TCP scaffolds fabricated at sintering temperatures of 950 °C and 1150 °C. Without using the structural compliance method, the corner region of the 1150 °C sintered scaffold had a statistically (p-value < 0.05) lower H and E_s than the edge and center regions. However, a large C_s was assessed in the corner region using the structural compliance method. After correcting H and E_s for the C_s, it was concluded that there were no statistically significant differences between regions. However, H and E_s in all regions increased significantly with sintering temperature.

Acknowledgments

The authors wish to thank Humberto Melgarejo for his contribution in sample preparation, Philips Plastic Corporation for providing the scaffolds and Hysitron Inc. for technical support during nano mechanical testing. JEJ acknowledges USDA Forest Service PECASE funding.

References

[1] R.Z. LeGeros, Calcium phosphate-based osteoinductive materials, Chem. Rev. 108 (11) (2008) 4742–4753.
[2] M. Vallet-Regí, J.M. González-Calbet, Calcium phosphates as substitution of bone tissues, Prog. Solid State Chem. 32 (1–2) (2004) 1–31.
[3] P. Kasten, I. Beyen, P. Niemeyer, R. Luginbühl, M. Bohner, W. Richter, Porosity and pore size of [beta]-tricalcium phosphate scaffold can influence protein production and osteogenic differentiation of human mesenchymal stem cells: an in vitro and in vivo study, Acta Biomater. 4 (6) (2008) 1904–1915.
[4] M. Riminucci, P. Bianco, Building bone tissue: matrices and scaffolds in physiology and biotechnology, Braz. J.Med. Biol. Res. 36 (2003) 1027–1036.
[5] H. Yuan, Z. Yang, Y. Li, X. Zhang, J.D. De Bruijn, K. De Groot, Osteoinduction by calcium phosphate biomaterials, J. Mater. Sci.: Mater. Med. 9 (12) (1998) 723–726.
[6] D.W. Hutmacher, Scaffolds in tissue engineering bone and cartilage, Biomaterials 21 (24) (2000) 2529–2543.
[7] S.V. Dorozhkin, Bioceramics of calcium orthophosphates, Biomaterials 31 (7) (2010) 1465–1485.
[8] L. Moroni, P. Habibovic, D.J. Mooney, V.B. C., Functional tissue engineering through biofunctional macromolecules and surface design, MRS Bull. 35 (8) (2010) 584–590.
[9] C.Y. Tang, P.S. Uskokovic, C.P. Tsui, D. Veljovic, R. Petrovic, D. Janackovic, Influence of microstructure and phase composition on the nanoindentation characterization of bioceramic materials based on hydroxyapatite, Ceram. Int. 35 (6) (2009) 2171–2178.
[10] C.X. Wang, X. Zhou, M. Wang, Influence of sintering temperatures on hardness and Young's modulus of tricalcium phosphate bioceramic by nanoindentation technique, Mater. Charact. 52 (4–5) (2004) 301–307.
[11] L.-H. He, O.C. Standard, T.T.Y. Huang, B.A. Latella, M.V. Swain, Mechanical behaviour of porous hydroxyapatite, Acta Biomater. 4 (3) (2008) 577–586.
[12] E. Hamed, I. Jasiuk, A. Yoo, Y. Lee, T. Liszka, Multi-scale modelling of elastic moduli of trabecular bone, J. R. Soc. Interface 9 (72) (2012) 1654–1673.
[13] U. Wolfram, H.-J. Wilke, P.K. Zysset, Valid μ finite element models of vertebral trabecular bone can be obtained using tissue properties measured with nanoindentation under wet conditions, J. Biomech. 43 (9) (2010) 1731–1737.
[14] N.M. Harrison, P.F. McDonnell, D.C. O'Mahoney, O.D. Kennedy, F. J. O'Brien, P.E. McHugh, Heterogeneous linear elastic trabecular bone modelling using micro-CT attenuation data and experimentally measured heterogeneous tissue properties, J. Biomech. 41 (11) (2008) 2589–2596.
[15] J. Zhang, G.L. Niebur, T.C. Ovaert, Mechanical property determination of bone through nano- and micro-indentation testing and finite element simulation, J. Biomech. 41 (2) (2008) 267–275.
[16] W.C. Oliver, G.M. Pharr, An improved technique for determining hardness and elastic modulus using load and displacement sensing indentation experiments, J. Mater. Res. 7 (6) (1992) 1564–1583.
[17] J.E. Jakes, D.S. Stone, The edge effect in nanoindentation, Philos. Mag. 91 (7–9) (2010) 1387–1399.
[18] J.E. Jakes, C.R. Frihart, J.F. Beecher, R.J. Moon, P.J. Resto, Z. H. Melgarejo, O.M. Suárez, H. Baumgart, A.A. Elmustafa, D.S. Stone, Nanoindentation near the edge, J. Mater. Res. 24 (3) (2009) 1016–1031.
[19] J.E. Jakes, C.R. Frihart, J.F. Beecher, R.J. Moon, D.S. Stone, Experimental method to account for structural compliance in nanoindentation measurements, J. Mater. Res. 23 (4) (2008) 1113–1127.
[20] D.S. Stone, K.B. Yoder, W.D. Sproul, Hardness and elastic modulus of TiN based on continuous indentation technique and new correlation, J. Vac. Sci. Technol. A: Vac., Surf. Films 9 (4) (1991) 2543–2547.
[21] S.-J.L. Kang, Sintering densification, Grain Growth Microstruct. (2005).
[22] F. Pecqueux, F. Tancret, N. Payraudeau, J.M. Bouler, Influence of microporosity and macroporosity on the mechanical properties of biphasic calcium phosphate bioceramics: modelling and experiment, J. Eur. Ceram. Soc. 30 (4) (2010) 819–829.

[23] J. Vivanco, A. Aiyangar, A. Araneda, H.-L. Ploeg, Mechanical characterization of injection-molded macro porous bioceramic bone scaffolds, J. Mech. Behav. Biomed. Mater. 9 (2012) 137–152.
[24] P. Habibovic, K. de Groot, Osteoinductive biomaterials—properties and relevance in bone repair, J.Tissue Eng. Regen. Med. 1 (1) (2007) 25–32.
[25] M. Bohner, Y. Loosli, G. Baroud, D. Lacroix, Commentary: deciphering the link between architecture and biological response of a bone graft substitute, Acta Biomaterialia 7 (2) (2011) 478–484.
[26] M.U. Entezarian, R.U. Smasal, J.C. Peskar, Methods, tools, and products for molded ordered porous structures, US Patent PCT/US2008/010218; 2009.
[27] J. Vivanco, J. Slane, R. Nay, A. Simpson, H.-L. Ploeg, The effect of sintering temperature on the microstructure and mechanical properties of a bioceramic bone scaffold, J. Mech. Behav. Biomed. Mater. 4 (8) (2011) 2150–2160.
[28] S.J. Kalita, R. Fleming, H. Bhatt, B. Schanen, R. Chakrabarti, Development of controlled strength-loss resorbable beta-tricalcium phosphate bioceramic structures, Mater. Sci. Eng. C 28 (3) (2008) 392–398.
[29] D.L. Joslin, W.C. Oliver, A new method for analyzing data from continuous depth-sensing microindentation tests, J. Mater. Res. 5 (1) (1990) 123–126.
[30] W.D. Nix, H. Gao, Indentation size effects in crystalline materials: a law for strain gradient plasticity, J. Mech. Phys. Solids 46 (3) (1998) 411–425.
[31] J. Vivanco, S. Garcia, E.L. Smith, H. Ploeg, Material and mechanical properties of tricalcium phosphate-based (TCP) scaffolds, in: Proceedings of the American Society of Mechanical Engineering (ASME) Summer Bioengineering Conference, Lake Tahoe, CA, 2009.